Ce6-conjugated, Gd-doped Gold Nanoclusters as Potential Theranostic Nanoplatform for Multi-modal Imaging-Guided Photodynamic Therapy

Qinghe Wu[1,a], Benchao Zheng[1,b], Pengli Zhang[1,c], Mengfei Hou[1,d], Yifei Jiang[1,e] and Chunfu Zhang[1,f,*]

[1]School of Biomedical Engineering, Shanghai Jiao Tong University, Shanghai 200030, China
a. wuqinghe@sjtu.edu.cn, b. 729721158@qq.com, c. plzhang2018@sjtu.edu.cn, d. houmf3@sjtu.edu.cn, e. 1060351923@qq.com, f. cfzhang@sjtu.edu.cn
**Chunfu Zhang*

Keywords: Gold nanoclusters, metal doping, theranostics, photodynamic therapy, magnetic resonance imaging, fluorescence imaging.

Abstract: Metal-doped gold nanoclusters have attracted considerable attention in biomedical applications due to their nontoxicity and unique doped metal-dependent physicochemical properties. Herein, gadolinium (Gd)-doped gold nanoclusters are fabricated by utilizing bovine serum albumin (BSA) as the stabilizing agent and chloride e6 (Ce6) as therapeutic molecules, respectively, *via* a simple one-pot synthesis approach. The obtained gold nanoclusters, Ce6@BSA-Au-Gd NCs, exhibit little dark toxicity to cells, and are able to serve as a multifunctional theranostic agent for dual-modal fluorescence and magnetic resonance (MR) imaging-guided photodynamic therapy (PDT). Gd-doping imparts the nanoparticles superior T1 magnetic resonance imaging (MRI) performance (r1= 12.32 $mM^{-1}s^{-1}$) compared with commercial MRI contrast agent (Gd-DTPA). In addition, the high cell internalization and large-capacity singlet oxygen ($^1O_2$) generation results in highly efficient PDT performance as revealed by ROS staining and cytotoxity assay in *vitro*. Collectively, we propose a successful paradigm for the design and preparation of theranostic nanoprobes based on metal-doped gold nanoclusters, which holds great potential in bioimaging and PDT-mediated cancer-killing applications.

1. Introduction

Compared to the conventional gold nanoparticles with large size (usually larger than 6 nm), ultra-small Au nanoclusters possess unique advantages for theranostic applications. For example, the discrete electron transitions resulting from the ultra-small size lead to some molecular-like properties like luminescence, making them be good candidates for fluorescence imaging agents. In order to endow gold nanoclusters good biocompatibility, various thiolated ligands such as peptides, DNA and

proteins were used as the capping molecues during the synthetic process [1, 2, 3]. Among these ligands, BSA exhibited advantages over other molecues, including biocompatibility and nontoxicity, as well as easy further functionalization by using its abundant amino acid residues [4].

Metal-doping gold nanoclusters demonstrated physicochemical-enhanced properties (optical, catalytical properties) compared to single gold nanoclusters [5, 6]. Furthermore, certain alloying metals contribute to new functions such as magnetic and photo-induced performance. Currently, there are two main strategies for doping metals in gold nanoclusters: (1) in situ synthesis by coreducing certain metals with gold precursors; (2) substituting a certain number of gold atoms from as-prepared gold nanoclusters with heteroatom complexes [7]. For instance, Negishi et al. synthesized Au-Ag nanoclusters with various proportions of Ag atoms, which showed different performance in optical spectra of Au nanoclusters [8]. Similar bi- or multimetallic metals-doping strategies (e.g., Pd, Pt, Cu, Cd and Hg) were also introduced and showed certain properties in varieties of applications [9, 10, 11].

Photodynamic therapy (PDT) as a noninvasive and direct local treatment strategy has shown great potential in both preclinical and clinical studies [12]. Ce6 as the most popular photosensitizers has been widely used as a PDT agent due to the easily conjugated property through hydrophobic interaction and amido linkages [13].

Herein, a facile synthesis route of theranostic nanoprobes based on BSA stabilized Au nanoclusters was proposed. Gadolinium was doped into gold nanoclusters through in situ coreduction method. The as-prepared Au-Gd nanoclusters showed enhanced fluorescence property and excellent magnetic resonance performance, making them one of the proper candidates for multi-modal imaging agents. Moreover, Ce6 was further loaded to the Au nanoclusters, which showed phototoxicity to MCF-7 cells upon illuminated by a 630nm laser. Our work demonstrated that Ce6-conjugated, Gd-doped Au nanoclusters were a robust theranostic nanoplatform for dual imaging-guided PDT.

2. Results and Discussion

2.1.Synthesis and Characterization of Ce6@BSA-Au-Gd NCs

BSA-Au NCs were synthesized according to a previously reported method with little modification [1], which took BSA as a stabilizer and reducing agent. Gd doping was performed by replacing a small portion of $HAuCl_4$ with $GdCl_3$ during synthesis. After BSA-Au-Gd NCs were synthesized, activated Ce6 was then conjugated to the particles through stable amido linkage by maintaining the reaction for another 2 h.

The final synthesized Ce6@BSA-AuGd NCs were purified and concentrated through ultrafiltration (Amicon, 3K) process to remove excess free Au^{3+} and Gd^{3+}. They were then characterized by dynamic light scattering (DLS), transmission electron microscopy (TEM), ultraviolet-visible (UV-Vis) spectroscopy and fluorescence spectra, etc. As shown in Figure 1 (a) and (b), DLS measurements and TEM images indicated that Ce6@BSA-AuGd NCs had a uniform size with a distribution of 3-5 nm, which was consistent with the previous reports [2]. UV-Vis absorption spectra showed that no absorption peak was detected around 500 nm (Figure 1 (c)), which was characteristic for ultra-small Au nanoparticles. Absorption spectra of BSA-Au-Gd NCs revealed that Gd doping slightly affects the electronic structure of Au nanoclusters (Figure 1 (d)), which resulted from the concentration of Au atoms. Ce6 was efficiently conjugated to the nanoclusters because the filtrate had very weak absorption peak at 504 nm and 655 nm, which were the characteristic absorption peaks of Ce6. The successful loading of Ce6 was also demonstrated through Zeta potential of Ce6@BSA-AuGd NCs before and after Ce6 conjugation (Figure 1 (e)). The fluorescence performance of as-prepared nanoprobes was tested by fluorescence spectrophotometer with

excitation wavelength of 507 nm (Figure 1 (f)), as shown in fluorescence curves, the Ce6 conjugated AuGd NCs showed strong emission peak around 668 nm, which had a 35 nm red shift and enhancement of fluorescence intensity compared to bare BSA-AuGd NCs that possessed an emission peak around 633 nm.

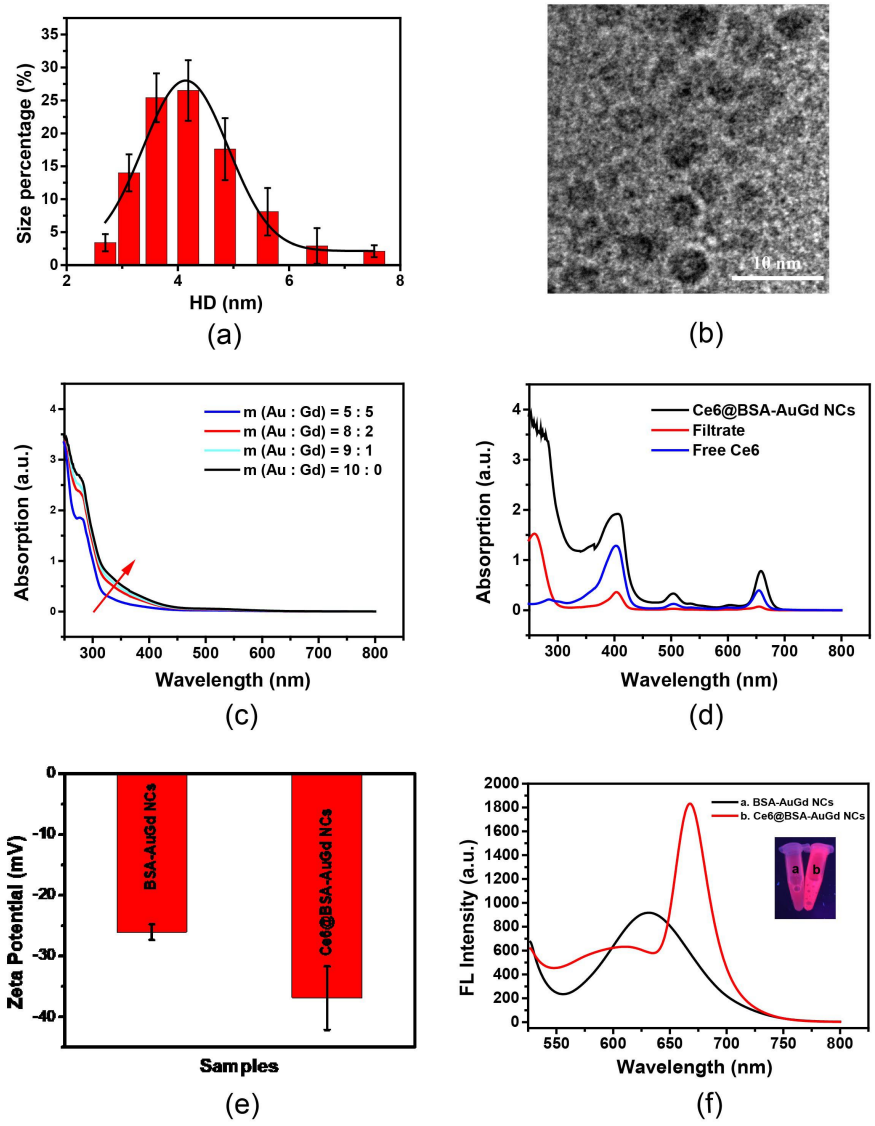

Figure 1: Characterizations of as-prepared nanoprobes. (a) DLS spectra and (b) Representative TEM images of Ce6@BSA-AuGd NCs. (c) UV-Vis spectra of BSA-AuGd NCs with Au-Gd molar ratio of 5: 5 (blue line), 8 : 2 (red line), 9 : 1 (green line) and 10 : 0 (BSA-Au NCs, black line). (d) UV-Vis spectra of purified Ce6@BSA-AuGd NCs (black line), filtrate (red line) and free Ce6 (blue line). (e) Zeta potential of BSA-AuGd NCs and Ce6@AuGd NCs. (f) Fluorescence spectra (with excitation wavelength of 507 nm) and photographs under UV light (365 nm) of BSA-AuGd NCs (a, black line) and Ce6@BSA-AuGd NCs (b, red line).

2.2.Magnetic Resonance Performance of BSA-Au-Gd NCs

To evaluate the potential magnetic resonance performance of the nanoprobes, the longitudinal relaxation times (T1) were measured with a 1.47 T NMR analyzer (Bruker mq60) at various concentrations of nanoprobes (0.025, 0.05, 0.067, 0.1, 0.2, 0.25, 0.5, 1.0 mM), in which Au-Gd

account as certain molar ratios (5:5, 8:2, 9:1, 10:0). It was found that by doping various number of Gd atoms, nanoprobes with different r1 values could be obtained and higher Gd to Au molar ratio contributed to enhanced r1 value, thus providing more efficient magnetic resonance performance. As illustrated in Figure 2, BSA-Au NCs without Gd doping showed no magnetic resonance property, yet BSA-AuGd NCs with 50% Gd doping exhibited high r1 value of 12.32 mM^{-1} s^{-1}, which was 3-4 times higher than that of commercial Magnevist Gd-DTPA,(r1=3.56 mM^{-1} s^{-1}) [14].

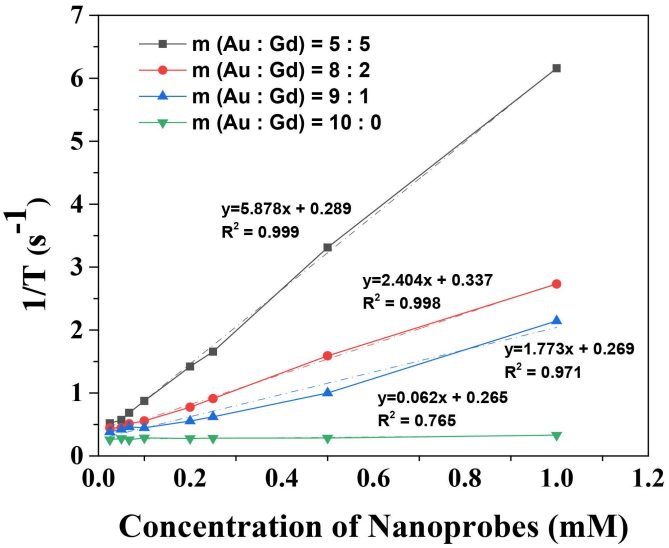

Figure 2: Longitudinal (T1) relaxation times of nanoprobes with various Au-Gd molar ratios (5:5: black line, 8:2: red line, 9:1: blue line, 10:0 (Au NCs): green line).

2.3.Singlet Oxygen ($^1O_2$) Generation of Nanoprobes

In order to detect singlet oxygen generated by Ce6@BSA-AuGd NCs, a singlet oxygen sensor green (SOSG) solution was introduced. SOSG solution was added into purified nanoprobes with a final concentration of 10 μM. After irradiation with 650 nm laser (40 mW cm^{-2}) for 5 min, the mixtures were then collected to measure the fluorescence performance. As shown in Figure 3 (a), the nanoprobes exhibited higher fluorescent intensity at 540 nm than control groups (water + SOSG, water + laser + SOSG) under the 650 nm laser irradiation, indicating the existence of $^1O_2$. The fluorescence intensity at 540 nm increased as extension of incubation time (30 min, 60 min, 90 min, 120 min) of nanoprobes with SOSG solution (Figure 3 (b)), demonstrating the continuous generation of $^1O_2$.

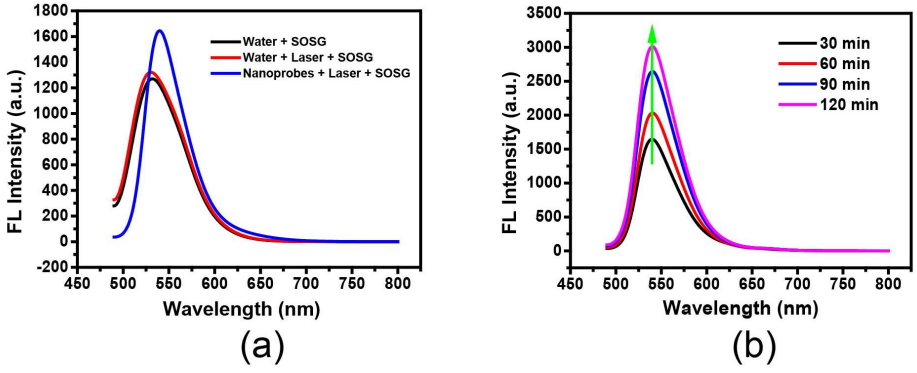

Figure 3: Detection of $^1O_2$ generated by Ce6@BSA-AuGd NCs through SOSG solution. (a) Fluorescence spectra of various materials after incubation with 10 µM SOSG solution for 30 min. (b) Changes of fluorescence intensity of 650 nm laser irradiated nanoprobes at different incubation time points (30 min, 60 min, 90 min, 120 min) with 10 µM SOSG solution.

2.4.Cellular Uptake and ROS Staining Assay

The intracellular ROS level could be detected by DCFH-DA staining. In order to evaluate the cellular uptake and efficiency of ROS generation by Ce6@BSA-AuGd NCs, MCF-7 cells were incubated with Ce6@BSA-AuGd NCs for 6 h and then irradiated by a 650 nm laser (40 mW cm^{-2}) for 3 min. The fluorescent images exhibited evident fluorescence signals from nanoprobes and DCF, indicating cellular uptake of nanoprobes and a high level of ROS generation *in vitro* (Figure 4). In contrast, there was no DCF fluorescence detected for the plain cells with or without laser exposure (Figure 4).

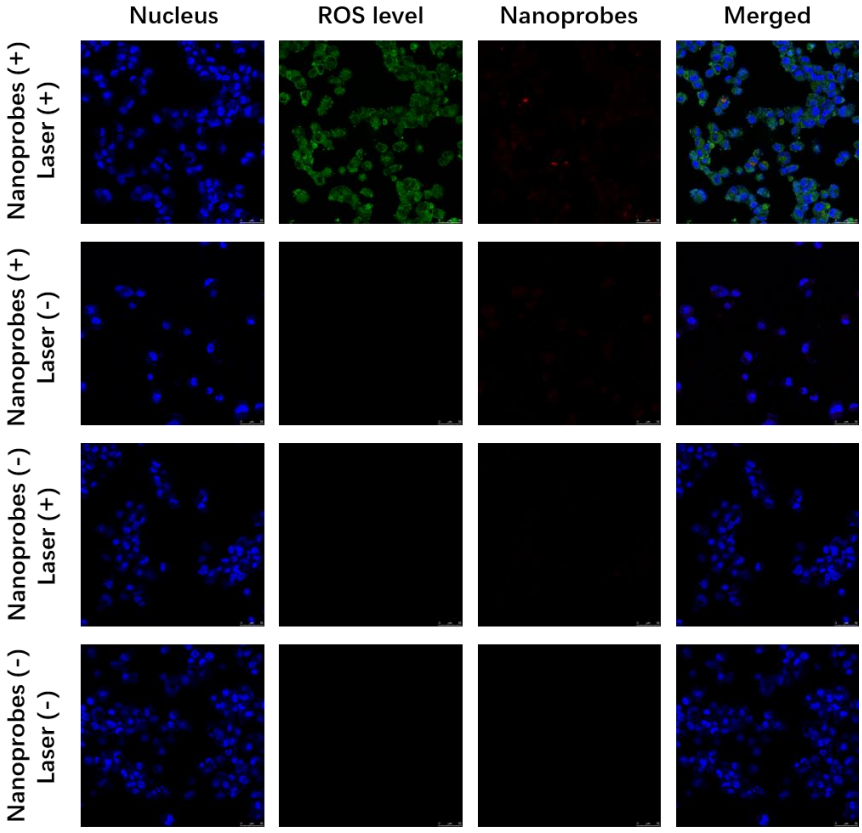

Figure 4: Cellular uptake assay through the red fluorescence of nanoprobes and measurement of the intracellular ROS levels by DCFH-DA staining.

2.5.Dark Toxicity and *in Vitro* PDT Efficacy of Nanoprobes

Excess ROS level causes damage to DNA, eventually leading to cell death. In order to evaluate the biocompatibility and cytotoxicity of Ce6@AuGd NCs, MCF-7 cells were exposed to various concentrations of nanoprobes for 24 h with/without 650 nm laser irradiation. There was no obvious dark cytotoxicity of nanoprobes even at a concentration of 8 µg Ce6/mL (Figure 5), indicating good biocompatibility of the nanoprobes. However, once irradiated by 650 nm laser (40 mW cm^{-2}) for 8 min, Ce6@BSA-AuGd NCs exhibited evident cytotoxicity, inducing the death of cells. Accordingly, the cell viability was only 39% at a concentration of 8 µg Ce6/mL with laser irradiation, which demonstrated the potential PDT of Ce6@AuGd NCs.

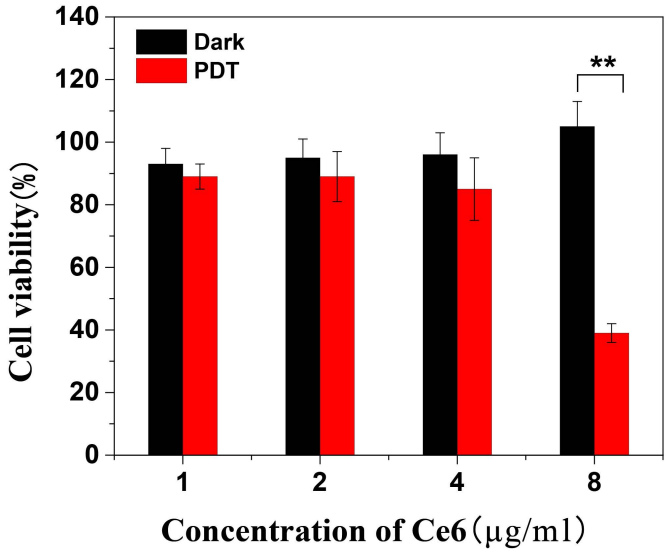

Figure 5: Test of dark toxicity (black columns) and phototoxicity (red columns) of Ce6@BSA-AuGd NCs through CCK-8 assay kit.

3. Conclusions

In summary, we reported an approach for preparation of multifunctional theranostic nanoprobes with dual-modal imaging-guided PDT. Gd atoms were doped into BSA-Au NCs with various of proportion through a facile in situ coreduction process. Ce6 was efficiently conjugated to the nanoclusters through amido bonds. The as-developed nanoprobes exhibited enhanced fluorescence around 670 nm and higher r1 relaxivity than Gd-DTPA. Once irradiated by 650 nm laser, Ce6@BSA-AuGd NCs showed efficacy of PDT on MCF-7 cells. Therefore, the design of nanoprobes described here provides a versatile yet effective paradigm for developing potential theranostic nanoprobes through metal-doping and bioactive surface modification of gold nanoclusters.

Acknowledgments

This study was supported by the National Natural Science Foundation of China (81571729, 81772338, 81930069), Innovation Research Plan supported by Shanghai Municipal Education Commission (2019-01-07-00-02-E00064, ZXWF082101) and Med-Engineering Crossing Foundation from Shanghai Jiao Tong University (YG2017ZD05).

References

[1] Zhang, X.D., Z. Luo, J. Chen, X. Shen, S. Song, Y. Sun, S. Fan, F. Fan, D.T. LeongJ. Xie, Ultrasmall Au(10-12)(SG)(10-12) nanomolecules for high tumor specificity and cancer radiotherapy, Adv. Mater. 26 (2014) 4565-4568.

[2] Chu, Z.Y., L.N. Chen, X.S. Wang, Q.Y. Yang, Q. Zhao, C.S. Huang, Y.K. Huang, D.P. YangN.Q. Jia, Ultrasmall Au-Ag Alloy Nanoparticles: Protein-Directed Synthesis, Biocompatibility, and X-ray Computed Tomography Imaging, Acs Biomaterials Science & Engineering. 5 (2019) 1005-1015.

[3] Wang, H.-B., H.-Y. Bai, A.-L. MaoY.-M. Liu, Poly(adenine) DNA-Templated Gold Nanocluster-Based Fluorescent Strategy for the Determination of Thiol-Containing Pharmaceuticals, Analytical Letters. 52 (2019) 2300-2311.

[4] Chen, Y.N., P.C. Chen, C.W. Wang, Y.S. Lin, C.M. Ou, L.C. HoH.T. Chang, One-pot synthesis of fluorescent BSA-Ce/Au nanoclusters as ratiometric pH probes, Chem. Commun (Camb). 50 (2014) 8571-8574.

[5] Krishnadas, K.R., T. Udayabhaskararao, S. Choudhury, N. Goswami, S.K. PalT. Pradeep, Luminescent AgAu Alloy Clusters Derived from Ag Nanoparticles - Manifestations of Tunable AuI-CuIMetallophilic Interactions, European Journal of Inorganic Chemistry. 2014 (2014) 908-916.

[6] Qian, H., D.E. Jiang, G. Li, C. Gayathri, A. Das, R.R. GilR. Jin, Monoplatinum doping of gold nanoclusters and catalytic application, J. Am. Chem. Soc. 134 (2012) 16159-16162.

[7] Kang, X., H. ChongM. Zhu, Au25(SR)18: the captain of the great nanocluster ship, Nanoscale. 10 (2018) 10758-10834.

[8] Negishi, Y., T. IwaiM. Ide, Continuous modulation of electronic structure of stable thiolate-protected Au25 cluster by Ag doping, Chem. Commun (Camb). 46 (2010) 4713-4715.

[9] Wang, S., Y. Song, S. Jin, X. Liu, J. Zhang, Y. Pei, X. Meng, M. Chen, P. LiM. Zhu, Metal exchange method using Au25 nanoclusters as templates for alloy nanoclusters with atomic precision, J. Am. Chem. Soc. 137 (2015) 4018-4021.

[10] Lu, Y., C. Zhang, X. Li, A.R. Frojd, W. Xing, A.Z. ClayborneW. Chen, Significantly enhanced electrocatalytic activity of Au 25 clusters by single platinum atom doping, Nano Energy. 50 (2018) 316-322.

[11] Takano, S., S. ItoT. Tsukuda, Efficient and Selective Conversion of Phosphine-Protected (MAu8)(2+) (M = Pd, Pt) Superatoms to Thiolate-Protected (MAu12)(6+) or Alkynyl-Protected (MAu12)(4+) Superatoms via Hydride Doping, J. Am. Chem. Soc. 141 (2019) 15994-16002.

[12] Agostinis, P., K. Berg, K.A. Cengel, T.H. Foster, A.W. Girotti, S.O. Gollnick, S.M. Hahn, M.R. Hamblin, A. Juzeniene, D. Kessel, M. Korbelik, J. Moan, P. Mroz, D. Nowis, J. Piette, B.C. WilsonJ. Golab, Photodynamic therapy of cancer: an update, CA. Cancer. J. Clin. 61 (2011) 250-281.

[13] Khlebtsov, B., E. Tuchina, V. TuchinN. Khlebtsov, Multifunctional Au nanoclusters for targeted bioimaging and enhanced photodynamic inactivation of Staphylococcus aureus, RSC Advances. 5 (2015) 61639-61649.

[14] Zhang, B., H. Jin, Y. Li, B. Chen, S. LiuD. Shi, Bioinspired synthesis of gadolinium-based hybrid nanoparticles as MRI blood pool contrast agents with high relaxivity, Journal of Materials Chemistry. 22 (2012) 14494.